11994 *Biochemistry* **2009,** *48,* 11994–12004
DOI: 10.1021/bi9014133

BIOCHEMISTRY
including biophysical chemistry & molecular biology
Article

Impact of Sugar Pucker on Base Pair and Mispair Stability†

Adides A. Williams, Agus Darwanto, Jacob A. Theruvathu, Artur Burdzy, Jonathan W. Neidigh, and Lawrence C. Sowers*

Department of Basic Sciences, School of Medicine, Loma Linda University, Loma Linda, California 92350

Received August 12, 2009; Revised Manuscript Received November 4, 2009

ABSTRACT: The selection of nucleoside triphosphates by a polymerase is controlled by several energetic and structural features, including base pairing geometry as well as sugar structure and conformation. Whereas base pairing has been considered exhaustively, substantially less is known about the role of sugar modifications for both nucleotide incorporation and primer extension. In this study, we synthesized oligonucleotides containing 2′-fluoro-modified nucleosides with constrained sugar pucker in an internucleotide position and, for the first time, at a primer 3′-end. The thermodynamic stability of these duplexes was examined. The nucleoside 2′-deoxy-2′-fluoroarabinofuranosyluracil [$U^{2'F(ara)}$] favors the 2′-endo conformation (DNA-like), while 2′-deoxy-2′-fluororibofuranosyluracil [$U^{2'F(ribo)}$] favors the 3′-endo conformation (RNA-like). Oligonucleotides containing $U^{2'F(ara)}$ have slightly higher melting temperatures (T_m) than those containing $U^{2'F(ribo)}$ when located in internucleotide positions or at the 3′-end and when correctly paired with adenine or mispaired with guanine. However, both modifications decrease the magnitude of $\Delta H°$ and $\Delta S°$ for duplex formation in all sequence contexts. In examining the thermodynamic properties for this set of oligonucleotides, we find entropy−enthalpy compensation is apparent. Our thermodynamic findings led to a series of experiments with DNA ligase that reveal, contrary to expectation based upon observed T_m values, that the duplex containing the $U^{2'F(ribo)}$ analogue is more easily ligated. The 2′-fluoro-2′-deoxynucleosides examined here are valuable probes of the impact of sugar constraint and are also members of an important class of antitumor and antiviral agents. The data reported here may facilitate an understanding of the biological properties of these agents, as well as the contribution of sugar conformation to replication fidelity.

The accurate replication of nucleic acids requires that polymerases select the correct nucleotide at each successive step of replication. Substantial work has focused on the importance of "base pairing fidelity" in the selection of the correct nucleotide (*1*−*6*). Polymerases must also choose among potential nucleoside triphosphates, even when the base pairing condition has been met. For example, RNA polymerases select ribonucleotide triphosphates (rNTPs), whereas DNA polymerases select 2′-deoxyribonucletide triphosphates (dNTPs) upon the basis of sugar structure and conformation. The selection of nucleotide triphosphates (NTPs) on the basis of differences in sugar structure and conformation has led to a suggested role for "sugar fidelity" among polymerases, although the mechanisms have not been extensively explored (*7*−*10*).

For a given DNA sequence position, polymerase discrimination must occur in two distinct steps. In the insertion step, a candidate nucleotide is interrogated for its capacity to bind to the primer−template−enzyme complex with sufficient stability in an acceptable geometry (*1*−*6*). Differences in the base pairing and base stacking energy between correct and incorrect nucleotides, as measured in oligonucleotide melting studies, have been proposed to account for polymerase discrimination at the insertion step. Following insertion, the polymerase must select the next correct nucleotide during the extension step. Surprisingly, polymerase extension beyond a mispair is very difficult, even for the insertion of a correct NTP and even though base pairing and geometry conditions are met (*11*−*15*). Extension fidelity contributes nearly as much to the overall replication fidelity as the initial insertion step. Although polymerase pausing at the extension step following a nucleotide misinsertion event would reduce the overall mutation frequency by facilitating proofreading or other repair, the mechanistic basis for extension fidelity is unknown.

Polymerase insertion and extension require a terminal 3′-hydroxyl (3′-OH) in the correct position to attack the α-phosphate of a candidate NTP. In the case of geometrically aberrant base pairs, such as a purine-purine mispair, the 3′-OH would be shifted several angstroms from the correct position, potentially preventing polymerase extension. With purine-pyrimidine mispairs, however, the geometry is closer to that of a normal Watson−Crick base pair, so that more subtle differences, such as sugar conformation, might become important. The furanose sugar component of nucleic acids is nonplanar and adopts a number of potential conformations that can be described by the pseudorotation angle, *P* (*16*−*18*). There are several conformations that correspond to energy minima as a function of *P*, and the value of *P* can significantly change the position of the 3′-OH. Ribonucleotides in RNA are biased toward a 3′-endo conformation, whereas 2′-deoxynucleosides in DNA assume preferentially a 2′-endo pucker, potentially explaining, in part, polymerase sugar fidelity (Figure 1).

While sugar conformation can be biased by sugar structure, sugar conformation can also be influenced by base pair configuration. Sugar conformation, and therefore 3′-OH position, can

†This work is supported by the National Institutes of Health, National Institute of General Medical Sciences (GM451336).

*To whom correspondence should be addressed. Telephone: (909) 558-4480. Fax: (909) 558-4035. E-mail: lsowers@llu.edu.

 Published on Web 11/09/2009

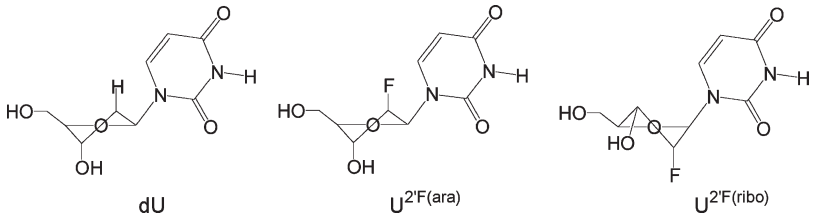

FIGURE 1: Nucleoside analogues examined in this study.

change because of mispair formation, as well as because of changes in the glycosidic torsion angle (*19*−*23*). While a correct base pair at the 3′-end of a template−primer complex would likely be found predominantly in a correct conformation with the 3′-OH in the correct position, mispair formation could modify sugar pucker and distort the position of the 3′-OH, potentially explaining, in part, polymerase extension fidelity.

Sugar conformation can also be biased by the presence of substituents in the furanose ring. The conformational difference between deoxyribose and ribose sugars is attributed primarily to the presence of the 2′-OH in the ribonucleosides. Other substituents, in particular, electron-withdrawing substituents including fluorine, are known to profoundly influence sugar conformation (*24*−*33*). Evidence that sugar pucker can influence both nucleotide incorporation and extension by polymerases exists (*34*−*41*). Nucleotides that are constrained to a 3′-endo conformation, for example, 2′-fluororibo nucleotides, are preferentially incorporated by RNA polymerases (*34*). Conversely, 2′-fluoroarabino nucleotides that prefer the 2′-endo pucker are preferentially incorporated by DNA polymerases yet, surprisingly, are very difficult to extend (*38*). The physical basis for this selectivity has not been established.

For this study, we constructed oligonucleotides with 2′-deoxyuridine (dU)[1] and the 2′-fluoro analogues 2′-deoxy-2′-fluoroarabinofuranosyluracil [$U^{2'F(ara)}$] and 2′-deoxy-2′-fluororibofuranosyluracil [$U^{2'F(ribo)}$] in both internucleotide and 3′-end positions (Figure 1). The sugar pucker equilibrium for the $U^{2'F(ara)}$ and $U^{2'F(ribo)}$ analogues studied here has been previously studied by NMR spectroscopy (*25*−*32*). The reference nucleoside analogue, dU, is in a rapid equilibrium between 2′-endo and 3′-endo conformations, with a preference (61%) for the 2′-endo conformation (*32*). The $U^{2'F(ara)}$ analogue is 57% 2′-endo, whereas the $U^{2'F(ribo)}$ analogue is 69% 3′-endo (*33*). When they are located in oligonucleotides and constrained by internucleotide linkages, the conformational preference of dU and $U^{2'F(ara)}$ shifts more toward 2′-endo whereas that of $U^{2'F(ribo)}$ shifts more toward 3′-endo (*26*).

The analogues described here were incorporated into an internucleotide position, as well as on the 3′-end. While both analogues have been incorporated previously into internucleotide positions, this is the first report of incorporation into the 3′-position. The analogues have been incorporated into duplex structures either properly paired with adenine or mispaired with guanine in an internucleotide position, as well as at a 3′-end position creating a model polymerase replication fork or ligase junction. The thermal and thermodynamic stability of these duplex structures has been studied. With this set of analogues, we could probe the energetic advantage or penalty for each analogue and base pair, as well as probe for a potential interaction between base pairing and sugar conformation. Thermodynamic results reported here led to a series of experiments with DNA ligase that demonstrate, unexpectedly, that the duplex containing the $U^{2'F(ribo)}$ analogue is more easily ligated. The thermodynamic parameters and results obtained are discussed within the context of the available literature on polymerase preferences for both nucleotide insertion and extension. Because of the importance of sugar-modified nucleosides as anticancer and antitumor drugs, the results reported here may provide new insight into the mechanisms of activity and the potential adverse effects of these analogues.

[1]Abbreviations: T_m, melting temperature; dU, 2′-deoxyuridine; $U^{2'F(ara)}$, 2′-deoxy-2′-fluoroarabinofuranosyluracil; $U^{2'F(ribo)}$, 2′-deoxy-2′-fluororibofuranosyluracil; araC, 1-β-D-arabinofuranosylcytosine.

MATERIALS AND METHODS

Materials. The solvents dichloromethane (CH_2Cl_2), methanol (MeOH), ethyl acetate (EtOAc), and hexanes were purchased from Fisher Scientific (Pittsburgh, PA). Pyridine, triethylamine (TEA), and acetonitrile (MeCN) were purchased from Sigma-Aldrich (St. Louis, MO). Dimethoxytrityl chloride (DMT-Cl) and 2-cyanoethyl tetraisopropyl phosphorodiamidite were purchased from Sigma-Aldrich. 1,3,5-Tri-*O*-benzoyl-2′-deoxy-2′-fluoro-D-arabinofuranose was purchased from MP Biomedicals (Aurora, OH). Thin layer chromatography (TLC) was performed on precoated silica gel 60 F_{254}, 5 cm × 20 cm, 250 μm thick plates purchased from EMD (Gibbstown, NJ).

Synthesis of 5′-Dimethoxy-2′-deoxy-2′-fluoro-1-β-D-arabinofuranosyluracil, 3′-[(2-Cyanoethyl)(N,N-diisopropyl)]phosphoramidite. Commercially available 1,3,5-tri-*O*-benzoyl-2′-deoxy-2′-fluoro-D-arabinofuranose was brominated to the corresponding bromo sugar in 100% yield (*42*, *43*). The bromo sugar was then coupled to 2,4-bis-*O*-trimethylsilyluracil to give 1-β-D-(3,5-di-*O*-benzoyl-2-fluoroarabinofuranosyl)uracil as a solid residue (*44*). The dibenzoyl derivative was then deprotected to give 2′-deoxy-2′-fluoro-1-β-arabinofuranosyluracil [$U^{2'F(ara)}$] in a 30% yield (*45*). $U^{2'F(ara)}$ was then tritylated to give 5′-dimethoxytrityl-2′-deoxy-2′-fluoro-1-β-arabinofuranosyluracil in 48% yield and subsequently converted to its phosphoramidite derivative, 5′-dimethoxy-2′-deoxy-2′-fluoro-1-β-D-arabinofuranosyluracil, 3′-[(2-cyanoethyl)(*N*,*N*-diisopropyl)]-phosphoramidite in 49% yield (*46*).

Oligonucleotide Synthesis and Characterization. Standard oligonucleotide synthetic procedures (*47*) were used to produce oligonucleotides with normal and modified analogues, including dU, $U^{2'F(ara)}$, and $U^{2'F(ribo)}$ residues located at an internucleotide site. Oligonucleotide synthesis was conducted with a Gene Assembler Plus (Pharmacia LKB) automated DNA synthesizer. Oligonucleotides were deprotected with concentrated NH_3 (aqueous) at 60 °C for 24 h. In general, following synthesis and deprotection, oligonucleotides were purified by HPLC using a Hamilton PRP-1 column and a gradient from 10 to 40% MeCN in potassium phosphate buffer (10 mM, pH 6.8) and examined by matrix-assisted laser desorption ionization time-of-flight mass spectrometry (MALDI-TOF-MS). Oligonucleotides were then

detritylated with 80% aqueous acetic acid at room temperature for 30 min. Following detritylation, oligonucleotides were purified by high-performance liquid chromatography (HPLC) using a C-18 Vydac column and a gradient from 0 to 20% MeCN in water. Oligonucleotide purity was examined by MALDI-TOF-MS (*48*), and the free base composition was verified by HPLC, following enzymatic digestion (*49*) using a Supelcosil LC-18-S column and a gradient from 0 to 15% MeCN in water.

Synthesis of Oligonucleotides with 3′-Terminally Located 2′-Deoxyuridine Analogues. To insert dU, $U^{2'F(ara)}$, and $U^{2'F(ribo)}$ residues at the primer terminus, three synthetic approaches were investigated using the following universal supports available from Glen Research: (1) Glen UnySupport CPG 500, (2) Universal Support II, and (3) Universal Support III PS (*50*, *51*). In each of the three approaches, it was necessary to increase the coupling times to 10 min (from 3 min) for insertion of $U^{2'F(ara)}$ and $U^{2'F(ribo)}$ residues at the primer terminus. Following detritylation, the overall purity of the oligonucleotides produced using each of the three universal supports was determined by MALDI-TOF-MS and a denaturing polyacrylamide gel [20% (v/v) polyacrylamide and 8 M urea]. On the basis of MALDI-TOF-MS analysis, oligonucleotides synthesized using Universal Support III PS were more pure than those synthesized using Universal Support II or Glen UnySupport CPG 500. In particular, the mass spectra for oligonucleotides containing $U^{2'F(ara)}$ and $U^{2'F(ribo)}$ residues, produced using Universal Support III PS, revealed single peaks corresponding to the expected oligonucleotide masses. Following synthesis using Glen UnySupport CPG 500, several unidentified impurities in $U^{2'F(ara)}$-containing oligonucleotides (M − 50, 221, 307, 360, and 619) and in $U^{2'F(ribo)}$-containing oligonucleotides (M + 18 and M − 227) were observed. On the basis of purity assessment following gel electrophoresis, Universal Support III PS was again determined to produce more highly pure oligonucleotides. In all, synthesis using Universal Support III PS produced oligonucleotides in greater quantity and of higher purity and was thus used exclusively for subsequent syntheses of oligonucleotides with dU, $U^{2'F(ara)}$, and $U^{2'F(ribo)}$ residues at the 3′-end.

Assessment of Duplex Melting Behavior. Samples containing non-self-complementary oligonucleotides were prepared in buffer containing 0.1 M NaCl, 0.01 M sodium phosphate, and 0.1 mM EDTA (pH 7.0). Complexes were prepared by mixing equimolar amounts of interacting strands, and concentration-dependent T_m measurements were conducted with a total strand concentration (C_T) between 2 and 60 μM in cuvettes with path lengths between 1 and 10 mm. Molar extinction coefficients of oligonucleotides were calculated (*52*) to determine single-strand concentrations. Oligonucleotide melting temperatures (T_m) were determined using a Varian Cary 300 Bio UV−visible spectrophotometer (Varian, Walnut Creek, CA). Five temperature ramps were performed on each sample per run while the absorbance at 260 nm was observed: (1) from 12 to 90 °C at a rate of 0.5 °C/min, (2) from 90 to 12 °C at a rate of 0.5 °C/min, (3) from 12 to 90 °C at a rate of 0.5 °C/min, (4) from 90 to 12 °C at a rate of 0.5 °C/min, and (5) from 12 to 90 °C at a rate of 0.5 °C/min. The sample was held for 3 min when the temperature reached 90 °C and for 10 min when it reached 12 °C, and then the next cycle was started. Data were collected at 0.5 °C intervals while the temperature was monitored with a probe inserted into a cuvette containing only buffer. The T_m of each duplex was determined using Cary WinUV Thermal software (Varian). Theoretical T_m values for control duplexes (A·dU and G·dU) were determined (*53*, *54*) and compared against values obtained using Cary WinUV Thermal. Thermodynamic parameters for non-self-complementary duplexes were calculated in two ways: (1) averages from fits of individual melting curves at different concentrations using the van't Hoff calculation in Cary WinUV Thermal and (2) $1/T_m$ versus $\ln(C_T/4)$ plots fitted to the following equation for the non-self-complementary sequences examined here.

$$T_m^{-1} = \frac{R}{\Delta H^\circ} \ln\left(\frac{C_T}{4}\right) + \frac{\Delta S^\circ}{\Delta H^\circ} \quad (1)$$

Both methods assume a two-state model, and $\Delta C_p = 0$ for the transition equilibrium. The two-state approximation was assumed to be valid for sequences in which the ΔH° values derived from the two methods agreed within 15% (*54*). The ΔH° values derived from the two methods agree within 15%, indicating that the two-state approximation is valid for all other sequences employed in this study.

Ligase Assays. *Escherichia coli* DNA ligase was obtained from New England Biolabs (Ipswich, MA), and human DNA ligase III was obtained from Enzymax (Lexington, KY). Oligonucleotide 5′-end radiolabeling was performed using adenosine 5′-[γ-^{32}P]triphosphate ([γ-^{32}P]ATP) (MP Biomedical, Costa Mesa, CA) and T4 polynucleotide kinase (New England BioLabs) under conditions recommended by the enzyme supplier. Labeled mixtures were subsequently centrifuged through G-25 Sephadex columns (Roche Applied Science, Indianapolis, IN) to remove excess unincorporated nucleotide. Duplex oligonucleotides containing a ligase junction were generated by mixing the labeled single strand (5′-GGCCACGACGG-3′) with a 2-fold molar excess of the CTTTGCCCGAAX strand, where X is dU, $U^{2'F(ara)}$, or $U^{2'F(ribo)}$, and CCGTCGTGGCCATTCGGGCAAAG in the appropriate enzyme buffer as previously described (*55*). The *E. coli* DNA ligase buffer contained 30 mM Tris-HCl (pH 8.0), 4 mM $MgCl_2$, 1 mM DTT, 26 μM NAD^+, and 50 μg/mL BSA. The human DNA ligase III buffer contained 50 mM Tris-HCl (pH 7.5), 10 mM $MgCl_2$, 10 mM DTT, and 1 mM ATP. Annealing mixtures were heated at 95 °C for 5 min and then cooled slowly to room temperature. Standard *E. coli* DNA ligase assays were performed using 50 nM substrate with 500 nM *E. coli* DNA ligase in buffer, as described above, in a total volume of 10 μL at 16 °C for selected time periods. Substrates (50 nM) were incubated with 50 nM human DNA ligase III in buffer, as described above, in a total volume of 10 μL at 26.5 °C for selected time periods. The reactions were terminated via addition of an equal volume of Maxam−Gilbert loading buffer (98% formamide, 0.01 M EDTA, 1 mg/mL xylene cyanole, and 1 mg/mL bromophenol blue). Samples were denatured by being heated at 95 °C for 5 min and quickly placed on ice for 2 min before electrophoresis on 20% denaturing polyacrylamide gels (8 M urea). The bands corresponding to substrate and products were visualized and quantified using a Molecular Dynamics PhosphorImager (Molecular Dynamics, Sunnyvale, CA, now part of GE Healthcare) and quantified using ImageQuant. Reaction rate constants (k_{obs}) for ligation reactions were determined by fitting time course data to a single exponential [$y = a(1 - a^{-bx})$] using Sigma Plot 10.0, where a is the maximum product ratio and b is the reaction rate constant, k_{obs}.

RESULTS

Oligonucleotide Synthesis. The phosphoramidite analogue of $U^{2'F(ribo)}$ is commercially available; however, the corresponding

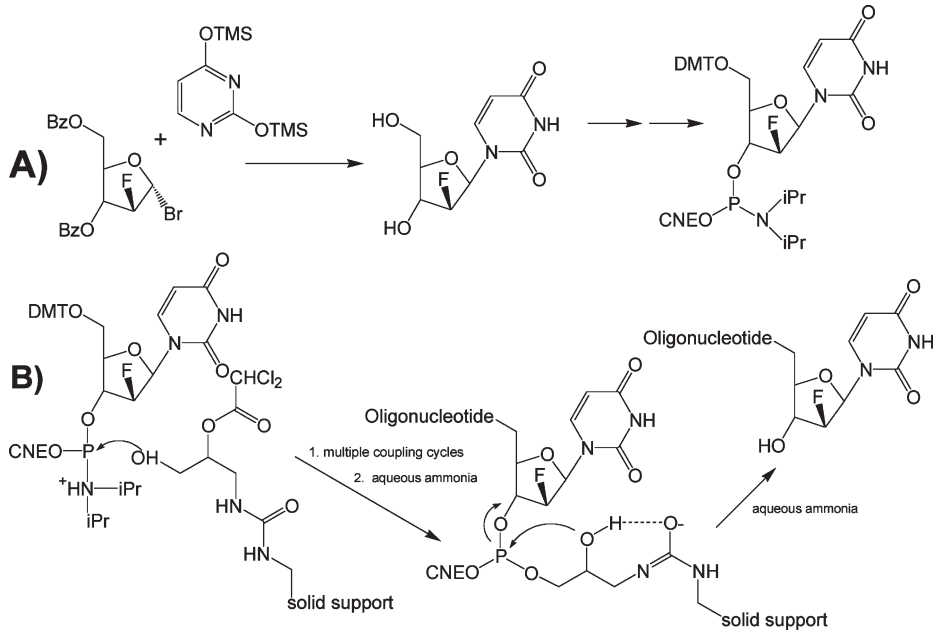

FIGURE 2: Oligonucleotide synthesis. (A) Abbreviated scheme showing the synthesis of phosphoramidites for the incorporation of $U^{2'F(ara)}$ into oligonucleotides. (B) Modified coupling conditions were used to attach $U^{2'F(ara)}$ to the 3′-terminus of oligonucleotides as described in Materials and Methods.

A 5′-CTTTGCCCGAAX-3′
3′-TAGGAAACGGGCTTPCAATAA-5′

B 5′-CCGAAXGTTATT-3′
3′-GGCTTPCAATAA-5′
X = dU, $U^{2'F(ara)}$, $U^{2'F(ribo)}$
P = A, G

C 5′-CTTTGCCCGAAX^{OH} ^{P}GGCCACGACGG-3′
3′-GAAACGGGCTTA-----CCGGTGCTGCC-5′

FIGURE 3: Oligonucleotide duplexes examined in this report. Sequences of duplexes with sugar-modified nucleotides at (A) the 3′-terminus or (B) an internucleotide position used in this report. (C) Sequences for oligonucleotide duplexes used as substrates for the ligase assays described in Materials and Methods.

phosphoramidite of $U^{2'F(ara)}$ is not available and was prepared in this laboratory by previously described methods as shown in Figure 2A. Oligonucleotides containing both analogues were prepared by standard solid phase synthesis methods. Sequences of oligonucleotides used in this study are shown in Figure 3.

Although the syntheses of oligonucleotides with $U^{2'F(ara)}$ and $U^{2'F(ribo)}$ have been previously reported, oligonucleotides with these analogues at the 3′-end are reported here for the first time. We considered two methods: the synthesis of solid phase supports linked to the analogues of interest or the use of solid supports containing linkers or "universal supports" for the preparation of 3′-end-modified oligonucleotides (Figure 2B). As the needed phosphoramidites were available in our lab, we proceeded to test a series of commercially available solid supports. Although we did not exhaustively examine all of the supports, we found that Universal Support III PS provided the highest consistent coupling yields and purity.

Oligonucleotide Characterization. Synthetic oligonucleotides were characterized by MALDI-TOF-MS following deprotection and purification by HPLC. The mass spectra of the oligonucleotides containing the $U^{2'F(ara)}$ analogue at both an internucleotide position and a 3′-end are shown in panels A and B of Figure 4, respectively. The observed mass in each case was consistent with the expected mass and demonstrated that the

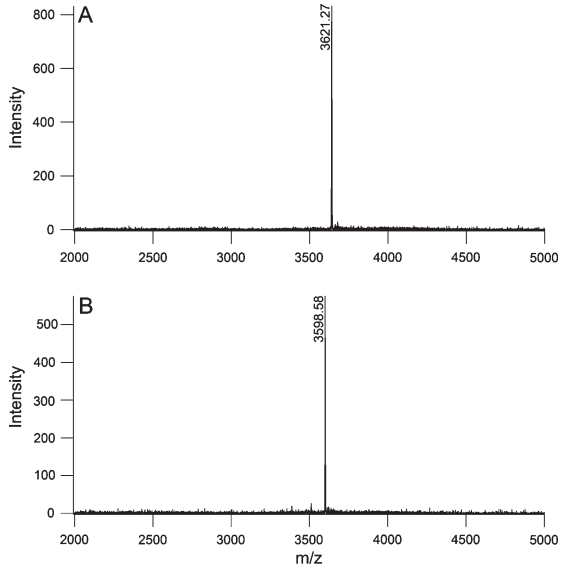

FIGURE 4: MALDI-TOF-MS spectra for $U^{2'F(ara)}$-containing oligonucleotides. (A) Mass spectrum observed for the oligonucleotide with the sequence 5′-CCGAA**X**GTTATT-3′, where **X** is a $U^{2'F(ara)}$ residue at an internucleotide site. (B) Mass spectrum observed for the oligonucleotide with the sequence 5′-CTTTGCCCGAA**X**-3′, where **X** is a $U^{2'F(ara)}$ residue at the 3′-end.

3′-phosphate of the original phosphoramidite had been removed (Figure 2B). Oligonucleotides were also characterized by enzymatic digestion and analysis of the liberated nucleosides by HPLC. We considered this important as the mass of the two 2′-fluoro analogues is identical, and we needed an additional method to confirm that the oligonucleotides contained the correct isomer. As shown in Figure 5A, dU, $U^{2'F(ara)}$, and $U^{2'F(ribo)}$ can be separated by HPLC and resolved from the standard DNA nucleosides (Figure 5B).

Measurement of Duplex Thermal and Thermodynamic Stability. Oligonucleotide duplexes were prepared in buffered solution by mixing equimolar amounts of the two strands,

as indicated in Figure 3. Strands were annealed by being heated to 90 °C, followed by slow cooling. Melting profiles were obtained by observing the UV absorbance at 260 nm as a function of temperature as described in Materials and Methods. Melting temperatures and corresponding thermodynamic parameters were obtained by analysis of the UV−temperature profiles as previously described (*53*, *54*). Melting temperatures and thermodynamic parameters are listed in Table 1. Example melting curves are shown in Figure 6.

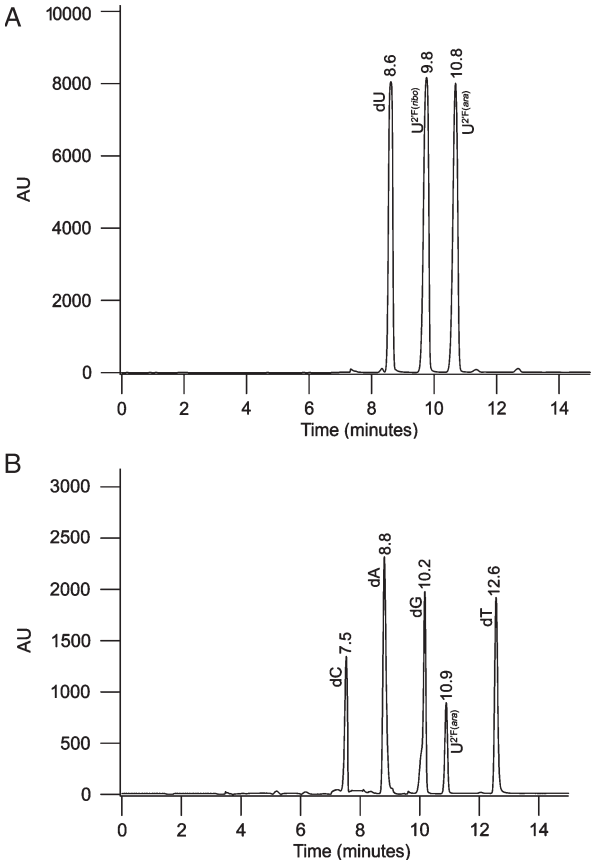

FIGURE 5: Composition of synthetic oligonucleotides analyzed by HPLC following enzymatic digestion. (A) HPLC was able to resolve the dU, $U^{2'F(ara)}$, and $U^{2'F(ribo)}$ nucleosides. (B) HPLC chromatogram confirming the composition of the oligonucleotide 5′-CCGA-A**X**GTTATT-3′, where X is a $U^{2'F(ara)}$ residue.

Analysis of Thermodynamic Data. Thermal and thermodynamic data obtained for the ensemble of oligonucleotides examined here were expressed as the corresponding differences by comparing the measured value for the substituted duplexes with the standard A·dU-containing duplex for the 3′-end and internucleotide series. These data and the corresponding values of ΔT_m, $\Delta\Delta G°_{37}$, $\Delta\Delta H°$, and $\Delta\Delta S°$ are listed in Table 1. Values of $\Delta\Delta H°$ and $\Delta\Delta S°$ appeared to correlate with one another, and this relationship is presented in Figure 7. Energy differences between base pairs examined in this study are shown diagrammatically in Figure 8.

DNA Ligase Activity. Oligonucleotides were assembled as shown in Figure 3C to create a ligase joint. The model ligase junction was incubated with human DNA ligase III and *E. coli* DNA ligase, and the reaction products were examined by gel electrophoresis as shown in Figure 9. Human DNA ligase III and *E. coli* DNA ligase were able to ligate junctions containing all three analogues. Human DNA ligase III was found to ligate junctions containing dU, $U^{2'F(ara)}$, and $U^{2'F(ribo)}$ with k_{obs} values of $(1.83 \pm 0.21) \times 10^{-2}$, $(4.70 \pm 0.43) \times 10^{-3}$, and $(2.18 \pm 0.25) \times 10^{-2}$ s^{-1}, respectively. In addition, *E. coli* DNA ligase was found to ligate junctions containing dU, $U^{2'F(ara)}$, and $U^{2'F(ribo)}$ with k_{obs} values of $(6.34 \pm 0.73) \times 10^{-3}$, $(8.64 \pm 1.33) \times 10^{-4}$, and $(2.81 \pm 0.39) \times 10^{-2}$ s^{-1}, respectively.

DISCUSSION

The Experimental Goal of This Study Was To Examine the Role of Constrained Sugar Pucker on Oligonucleotide Stability for both a Correct Base Pair and a Wobble Mispair in both Internucleotide and 3′-Terminal Positions. These properties might help explain why polymerases initially

Table 1: Experimental Thermodynamic Parameters of Duplex Formation[a]

	$\Delta G°_{37}$ (kcal/mol)	$\Delta\Delta G°_{37}$ (kcal/mol)	$T_{m28\mu M}$ (°C)	$\Delta T_{m28\mu M}$ (°C)	$\Delta H°$ (kcal/mol)	$\Delta\Delta H°$ (kcal/mol)	$\Delta S°$ (cal mol^{-1} K^{-1})	$\Delta\Delta S°$ (cal mol^{-1} K^{-1})
				3′-Terminal				
A·dU	−9.5 ± 0.2	–	49.4 ± 0.3	–	−89.0 ± 4.6	–	−251.2 ± 14.2	–
G·dU	−9.0 ± 0.2	**0.5 ± 0.3**	48.1 ± 0.2	−1.3 ± 0.4	−86.0 ± 5.4	3.0 ± 7.1	−244.2 ± 16.7	7.0 ± 21.9
A·$U^{2'F(ara)}$	−9.5 ± 0.2	0.0 ± 0.3	50.3 ± 0.1	0.9 ± 0.3	−84.8 ± 3.2	4.2 ± 5.6	−238.4 ± 9.7	12.8 ± 17.2
G·$U^{2'F(ara)}$	−8.8 ± 0.2	**0.7 ± 0.3**	48.1 ± 0.5	−1.3 ± 0.6	−82.1 ± 4.3	**6.9 ± 6.3**	−232.0 ± 13.4	19.2 ± 19.5
A·$U^{2'F(ribo)}$	−9.0 ± 0.2	**0.5 ± 0.3**	49.2 ± 0.2	−0.2 ± 0.4	−79.9 ± 3.9	**9.1 ± 6.0**	−224.3 ± 12.2	**26.9 ± 18.7**
G·$U^{2'F(ribo)}$	−8.6 ± 0.2	**0.9 ± 0.3**	47.2 ± 0.6	−2.2 ± 0.7	−76.7 ± 5.1	**12.3 ± 6.9**	−215.7 ± 15.8	**35.5 ± 21.2**
				Internucleotide				
A·dU	−8.1 ± 0.2	–	43.8 ± 0.2	–	−93.2 ± 5.1	–	−271.4 ± 14.9	–
G·dU	−6.2 ± 0.1	**1.9 ± 0.2**	36.6 ± 0.2	−7.2 ± 0.3	−87.1 ± 3.7	6.1 ± 6.3	−257.6 ± 12.4	13.8 ± 19.4
A·$U^{2'F(ara)}$	−8.0 ± 0.1	0.1 ± 0.2	43.8 ± 0.3	0.0 ± 0.4	−85.4 ± 3.0	**7.8 ± 5.9**	−245.7 ± 9.5	**25.7 ± 17.6**
G·$U^{2'F(ara)}$	−6.5 ± 0.1	**1.6 ± 0.2**	37.5 ± 0.2	−6.3 ± 0.3	−81.7 ± 3.7	**11.4 ± 6.3**	−239.6 ± 11.8	**31.9 ± 19.0**
A·$U^{2'F(ribo)}$	−7.8 ± 0.1	**0.3 ± 0.2**	42.9 ± 0.1	−0.9 ± 0.2	−86.7 ± 3.5	**6.4 ± 6.2**	−250.7 ± 11.1	**20.7 ± 18.6**
G·$U^{2'F(ribo)}$	−6.4 ± 0.1	**1.7 ± 0.2**	36.7 ± 0.5	−7.1 ± 0.5	−81.9 ± 2.9	**11.3 ± 5.8**	−240.2 ± 9.3	**31.2 ± 17.5**

[a]The values include the measured free energy of duplex formation ($\Delta G°_{37}$), enthalpy ($\Delta H°$), entropy ($\Delta S°$), and melting temperature with a strand concentration of 28 μM ($T_{m28\mu M}$). The thermodynamic parameters for the A·dU oligonucleotides were used as the references when calculating $\Delta\Delta G°_{37}$, $\Delta\Delta H°$, and $\Delta\Delta S°$ in the 3′-terminal (Figure 3A) or internucleotide positions (Figure 3B). Measured free energy, enthalpy, and entropy differences that exceed experimental error are indicated in bold.

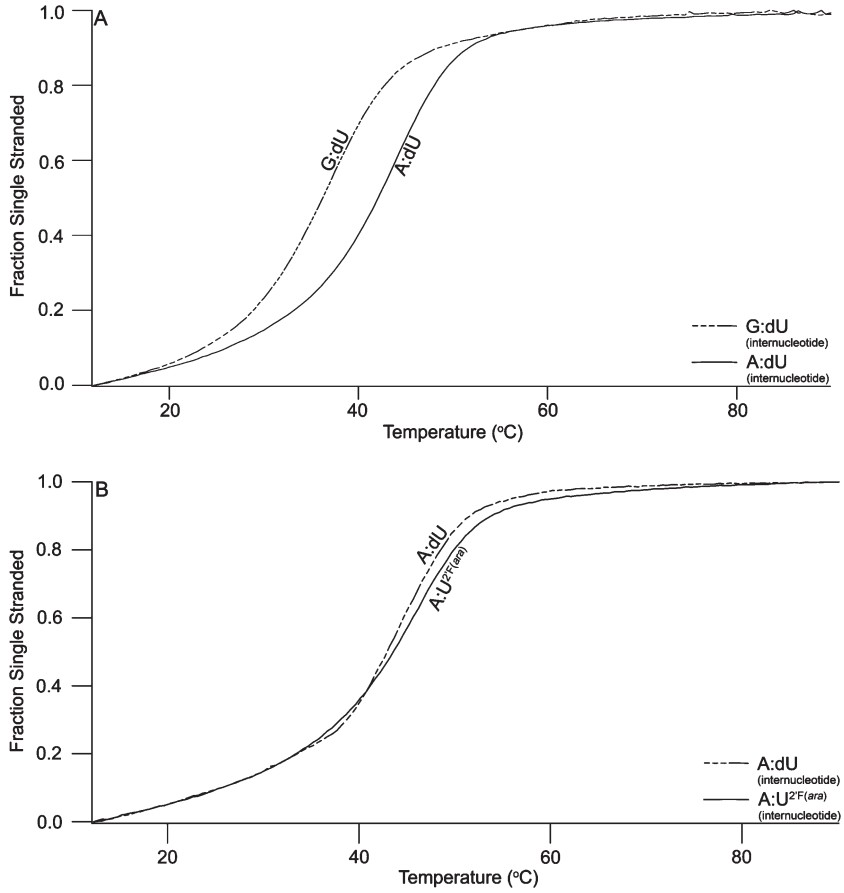

FIGURE 6: Ultraviolet melting curves of complexes at 28 (A) and 60 μM (B) in 100 mM NaCl, 0.1 mM EDTA, and 10 mM phosphate buffer (pH 7.0).

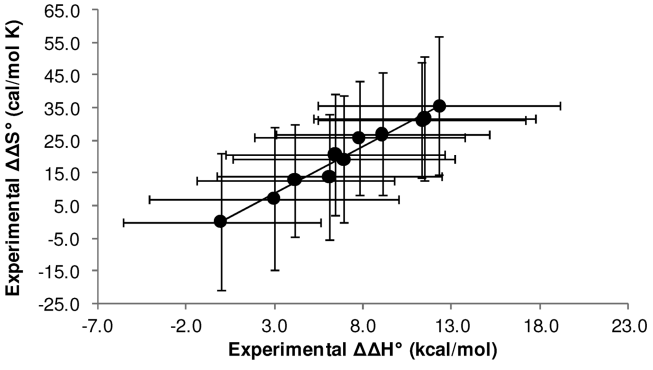

FIGURE 7: Thermodynamics of duplex formation display enthalpy−entropy compensation. The slope of the line is 2.9, and the R^2 value of the associated trend line is 0.98. Experimental $\Delta\Delta H°$ and $\Delta\Delta S°$ values are listed in Table 1.

insert correct nucleotides (insertion) and insert correct nucleotides following mispairs (extension) with such low efficiency. The impact of constrained sugar conformation on mispairs has not been previously examined. We considered the possibility that mispair geometry might be coupled with changes in sugar pucker at a duplex 3′-end which might help explain the inefficiency of mispair extension. Previous structural studies have suggested that aberrant base pair geometry could induce changes in sugar conformation (*19*−*23*); however, these effects have not been previously studied at a replication fork. The sugar-substituted nucleosides examined here are also members of an important class of nucleoside analogues with antitumor and antiviral properties (*34*−*41*), and thus, the data reported here might facilitate an improved understanding of the biological activity of this class of nucleoside analogues. Our experimental approach was to construct oligonucleotides containing dU and 2′-fluoro analogues constrained to either the 2′-endo (south, DNA-like) sugar pucker or the 3′-endo (north, RNA-like) sugar pucker and to measure thermodynamic stabilities of duplex oligonucleotides.

Melting Temperatures for Oligonucleotides Containing Standard and Modified Nucleotides Were Determined, and Measured Values Were Consistent with Expectations. In the studies reported here, uracil was selected as the pyrimidine rather than thymine so that the data set examined here could be used in future studies to compare a series of 5-substituted pyrimidines. The replacement of T with dU does not change base pairing geometry when paired with A (*56*) or mispaired with G (*57*) and results in only a modest decline in T_m due to a reduced level of base stacking (*58*). Oligonucleotide duplexes were assembled as shown in Figure 3. Oligonucleotide melting temperatures were obtained from the temperature dependence of the UV absorbance as shown in Figure 5. Thermodynamic parameters were extracted from the melting curves, and the corresponding data are presented in Table 1. The observed T_m of the duplex containing an internucleotide A·dU base pair was 43.8 ± 0.2 °C. The expected T_m for a duplex with the same sequence except with dU replaced with thymine is 43.8−44.2 °C, depending upon which basis set and method of calculation are used (*53*). The observed T_m of the duplex in which the dU residue on the 3′-end was paired with A was observed to be 49.4 ± 0.3 °C, slightly below the 52.8−53.1 °C calculated range when dU is replaced with T (*53*).

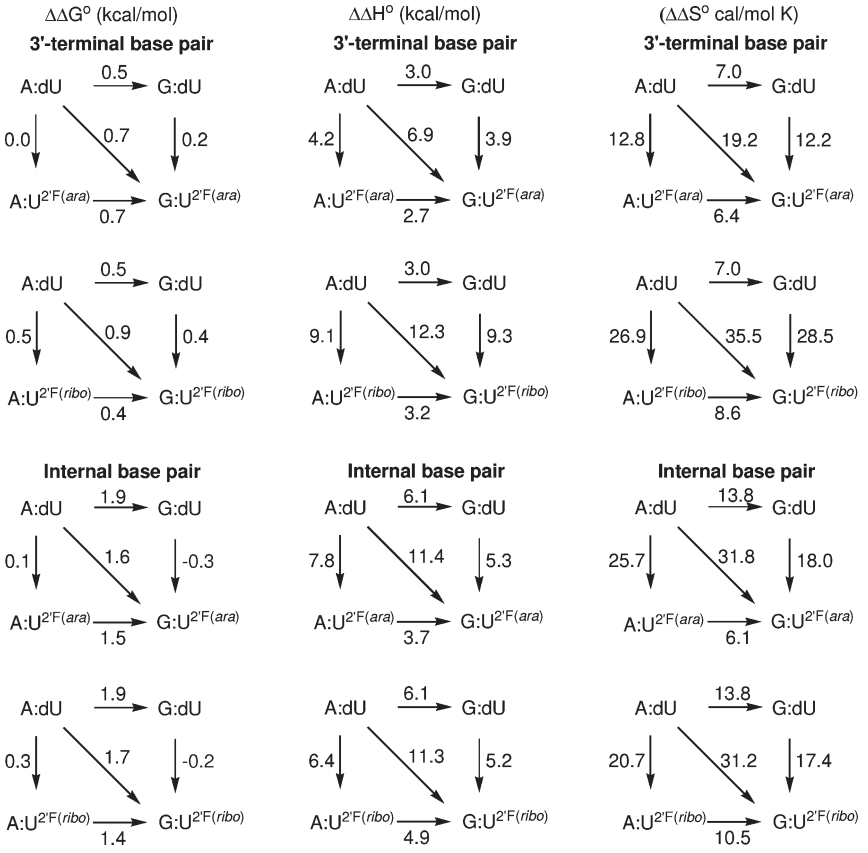

FIGURE 8: Comparison of the differences in free energy ($\Delta\Delta G°_{37}$), enthalpy ($\Delta\Delta H°$), and entropy ($\Delta\Delta S°$) between substituted duplexes and the standard A·dU-containing duplex. Numbers adjacent to arrows represent corresponding differences between duplexes. Values of $\Delta\Delta G°_{37}$, $\Delta\Delta H°$, and $\Delta\Delta S°$ for each duplex are listed in Table 1.

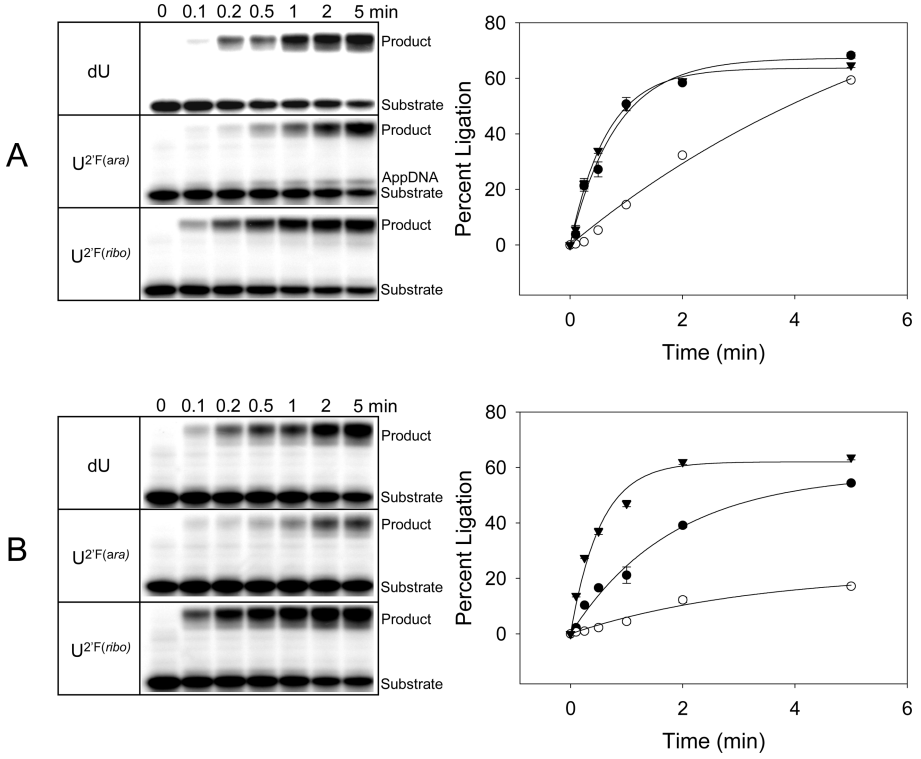

FIGURE 9: Ligase activities on 3′-terminal dU (●), $U^{2'F(ara)}$ (○), and $U^{2'F(ribo)}$ (▼) residues paired with adenine. (A) The experiments were performed at 26.5 °C with 50 nM substrate and 50 nM human DNA ligase III in a total volume of 10 μL. AppDNA indicates the 5′-AMP intermediate product of the ligation reaction. (B) The experiments were performed at 16 °C with 50 nM substrate and 500 nM *E. coli* DNA ligase in a total volume of 10 μL.

The conversion of a Watson−Crick base pair to a wobble mispair is known to significantly decrease melting temperatures (*1*, *11*, *58*). The formation of the internucleotide G·dU mispair results in a T_m of 36.6 ± 0.2 °C, 7.2 °C lower than that for the A·dU duplex. The calculated range for a duplex of the same sequence containing a G·dT mispair is 36.8−38.2 °C (*54*). When the G·dU mispair is moved from an internucleotide position to the 3′-end, the observed T_m is 48.1 ± 0.2 °C, only 1.3 °C lower than the T_m for the sequence containing a correct A·dU base pair. The expected T_m for an oligonucleotide of an otherwise same sequence, but with a G·dT rather than G·dU mispair at the 3′-end, is 50.2−50.8 °C (*54*). The data reported thus far are consistent with expectations based upon literature precedents and confirm that the impact of a mispair on T_m is substantially weaker when the mispair is located at the 3′-end.

The T_m of the duplex containing the internucleotide A·U$^{2'F(ara)}$ base pair is observed to be 43.8 ± 0.3 °C, experimentally indistinguishable from that of the A·dU duplex. Previously, other investigators have observed that the placement of 2′-fluoroarabino analogues in duplex structures increases their melting temperatures by roughly 1 °C per nucleotide, and this stabilizing effect has been attributed to constraining the sugar into the more DNA-like 2′-endo pucker (*28*, *32*). In most of the previous studies, however, the oligonucleotides included multiple substitutions. The observed T_m for the formation of the internucleotide G·U$^{2'F(ara)}$ mispaired duplex is 37.5 ± 0.2 °C, which is 0.9 °C higher than that of the G·dU duplex. The 3′-terminal A·U$^{2'F(ara)}$ base pair duplex exhibited a T_m 0.9 °C higher than that of the 3′-terminal A·dU base pair duplex, whereas the T_m of the terminal G·U$^{2'F(ara)}$ mispair duplex is indistinguishable from the T_m of the 3′-terminal G·dU duplex. These results demonstrate that incorporation of the U$^{2'F(ara)}$ analogue stabilizes duplexes in some cases; however, the observed effect on T_m is modest and substantially weaker than the impact of mispair formation.

Substitution of dU with the U$^{2'F(ribo)}$ analogue at an internucleotide position has the opposing effect, slightly decreasing T_m values when paired with A or mispaired with G. Again, the impact of the sugar constraint on T_m is weaker than that of mispair formation at the internucleotide position. At the 3′-end, the effect of the sugar constraint on T_m shows similar decreases. One of the initial hypotheses considered here is that mispair geometry might be related to sugar pucker at a duplex 3′-end, and therefore, a nucleotide with constrained sugar pucker might have an opposing impact on a mispair versus a normal pair. The evidence thus far on T_m values does not support this hypothesis in that mispairs with G are approximately 2 °C less stable than base pairs with A for both U$^{2'F(ara)}$ and U$^{2'F(ribo)}$ analogues.

Oligonucleotide Duplexes with Similar T_m Values Can Have Significantly Different Thermodynamic Parameters if Enthalpy and Entropy Changes Are Correlated. Although oligonucleotide duplexes might have similar T_m values, they can have different thermodynamic parameters. For this reason, we examined the free energy changes at 37 °C ($\Delta G°_{37}$), changes in enthalpy ($\Delta H°$), and changes in entropy ($\Delta S°$) for each of the duplex structures reported here (Table 1). In Figure 6B, the melting curves for oligonucleotides with A·dU and A·U$^{2'F(ara)}$ base pairs are shown. Although the midpoint for the temperature-dependent UV transition (T_m) is similar for each, the shapes of the curves, and corresponding thermodynamic parameters, are different. The magnitude of the experimental errors for $\Delta S°$, $\Delta H°$, and $\Delta G°$ observed here are in accord with previously reported studies (*58*, *60*).

To assess the impact of the substitution on the thermodynamic parameters, the free energy, enthalpy, and entropy changes are expressed as the corresponding differences ($\Delta\Delta G°$, $\Delta\Delta H°$, and $\Delta\Delta S°$, respectively) relative to the A·dU base pair for the internucleotide or 3′-terminal series. In all cases, positive values are observed for $\Delta\Delta G°_{37}$, $\Delta\Delta H°$, and $\Delta\Delta S°$, indicating that constraining the sugar pucker with either the U$^{2'F(ara)}$ or U$^{2'F(ribo)}$ analogue has a destabilizing effect, as does mispair formation. Previously, positive values for $\Delta\Delta H°$ and $\Delta\Delta S°$ upon substitution with U$^{2'F(ara)}$ have been observed (*25*), and the magnitudes of these changes per substitution are similar to those reported here. The impact of the sugar constraint on $\Delta\Delta S°$ has been attributed to a conformational preorganization, reducing the net conformational entropy change upon duplex formation (*25*). The impact on $\Delta\Delta H°$ would be attributed to the constrained sugar preventing the formation of the most favorable base stacking geometry.

In this study, we have assumed a two-state equilibrium between 2′-endo and 3′-endo sugar puckers as supported by previous NMR studies with the U$^{2'F(ara)}$ and U$^{2'F(ribo)}$ analogues studied here (*25*−*32*). The reference nucleoside analogue, dU, is in a rapid equilibrium between 2′-endo and 3′-endo conformations, with a preference (61%) for the 2′-endo conformation (*32*). The U$^{2'F(ara)}$ analogue is 57% 2′-endo, whereas the U$^{2'F(ribo)}$ analogue is 69% 3′-endo (*33*). When they are located in oligonucleotides and constrained by internucleotide linkages, the conformational preference of dU and U$^{2'F(ara)}$ shifts more toward 2′-endo whereas that of U$^{2'F(ribo)}$ shifts more toward 3′-endo (*26*).

Enthalpy and entropy differences for the oligonucleotide duplexes examined here are shown to be proportional. In previous studies of oligonucleotide stability in which mispairs and constrained sugar pucker were considered separately, enthalpy and entropy contributions were shown to correlate (*60*). As shown in Figure 7, enthalpy and entropy are shown to correlate for the series examined here, as well. The relatively large size of the error bars when the values are presented as $\Delta\Delta S°$ and $\Delta\Delta H°$ is consistent with previous studies as discussed by McTigue et al. (*60*). The slope of the line in Figure 7 is 2.9, and this plot includes normal base pairs, those with sugar constraints and unconstrained mispairs, and mispairs with sugar constraints in both internucleotide and 3′-terminal positions. This value compares favorably with the value of 2.8 from a previous study on mispairs with no sugar constraint (*11*) and with the value of 2.95 from a study that examined constrained sugars but no mispairs (*60*), suggesting that this value of $\Delta\Delta S°/\Delta\Delta H°$ is broadly applicable to nucleic acids.

Thermodynamic Differences for 3′-End Base Pairs Likely Contribute to Polymerase Insertion Kinetics. Previous studies have established that sugar pucker can also influence nucleotide insertion by DNA polymerases. DNA polymerases must distinguish between NTPs with different sugars, and it is known that the discrimination is between 1 and 3 orders of magnitude depending upon the template and polymerase; several apparent K_m values have been reported. Astatke et al. (*9*) demonstrated that the mechanism for discrimination by *E. coli* DNA polymerase between deoxy- and dideoxynucleotides involves a direct interaction with the 3′-OH present on the deoxynucleotide, but not the dideoxynucleotide, accounting for a K_m several orders of magnitude higher for the dideoxynucleotide. Richardson et al. (*8*) demonstrated that human polymerase α and polymerase γ accept U$^{2'F(ara)}$ nucleotides with K_m values similar to that of dUTP. However, both

polymerases discriminate against ribonucleotides and 2′-deoxy-2′-fluororibonucleotides with K_m values that are increased between 1 and 2 orders of magnitude, although all of these nucleotides contain the necessary 3′-OH.

Previously, Goodman and co-workers (*11*) explained how polymerases could discriminate against mispairs by amplifying free energy differences ($\Delta\Delta G°$) between correct and incorrect base pairs. Free energy differences are determined by the relative magnitude of the enthalpy and entropy contributions ($\Delta\Delta G° = \Delta\Delta H° - T\Delta\Delta S°$). If $\Delta\Delta H°$ and $\Delta\Delta S°$ are proportional, large values of $\Delta\Delta H°$ might be offset by large values of $\Delta\Delta S°$, giving small values of $\Delta\Delta G°$. On the other hand, if the polymerase active site accepts only nucleotides with sugar conformations that approximate the correct conformations, $\Delta\Delta G°$ would approach $\Delta\Delta H°$, providing sufficient energy for the observed discrimination. One of the surprising findings of this study is that, despite modest differences in T_m ($\Delta T_m = -0.2$ °C), the measured difference in free energy change between A·dU and A·$U^{2'F(ribo)}$ base pairs ($\Delta\Delta G° = 0.5$ kcal/mol) is as large as the corresponding difference in free energy change between a correct A·dU base pair and a G·dU mispair ($\Delta\Delta G° = 0.5$ kcal/mol), although the mispair has a substantially larger impact on the observed T_m ($\Delta T_m = -1.3$ °C). These results are consistent with a thermodynamic contribution to sugar fidelity for polymerase insertion.

Thermodynamic Differences Resulting from Mispair Formation and Sugar Constraint Appear To Be Additive in All Cases, Suggesting That Sugar Conformation and Mispair Geometry Are Independent and Not Interacting. Our initial expectation was that constraining the sugar pucker to 2′-endo [$U^{2'F(ara)}$] would stabilize a correct base pair but destabilize an incorrect base pair, whereas the 3′-endo sugar [$U^{2'F(ribo)}$] would destabilize the correct base pair and stabilize the mispair. Our experimental results are inconsistent with this expectation. When the impact of mispair formation and sugar pucker on $\Delta\Delta G°$ is examined, the contributions of each appear to be additive for both 3′-terminal and internucleotide positions. Neither constrained pucker appears to selectively stabilize or destabilize either the correct base pair or the mispair, in accord with observations of T_m discussed above. The contributions of mispair formation and constrained sugar pucker also appear to be additive for $\Delta\Delta H°$ and $\Delta\Delta S°$ in all cases presented here, as indicated in Figure 8. For example, for the internucleotide A·dU base pair, conversion to a G·dU mispair is associated with a $\Delta\Delta H°$ of 6.1 kcal/mol. The energy penalty associated with constraining the sugar conformation of the mispairs by comparing G·dU and G·$U^{2'F(ara)}$ is associated with a $\Delta\Delta H°$ of 5.3 kcal/mol. The combined effect of mispair formation and constraining the sugar with the $U^{2'F(ara)}$ analogue would be expected to be 11.4 kcal/mol if they were additive and not interacting, which is the observed value obtained upon comparison of the thermodynamic properties of the A·dU and G·$U^{2'F(ara)}$ duplexes.

The observation that the influences of mispair geometry and sugar constraint are simply additive strengthens the proposal that aberrant base pair geometry and constrained sugar pucker are not linked. Therefore, it is unlikely that the altered base pairing geometry of a mispair induces a shift in equilibrium for the 3′-residue, placing the 3′-OH in a position inconsistent with insertion of the next nucleotide. The data presented thus far suggest that polymerases are unlikely to exploit induced changes in sugar conformation to increase replication fidelity.

Net Thermodynamic Differences between 3′-End-Modified Duplexes and Internally Modified Duplexes Might Explain Why Polymerase Extension beyond a Mispair Is So Difficult. The magnitudes of the observed $\Delta\Delta H°$ and $\Delta\Delta S°$ values for the 3′-terminal G·dU mispairs are 3.0 kcal/mol and 7.0 cal mol^{-1} K^{-1}, respectively, whereas for the internucleotide mispair, the values increase to 6.1 kcal/mol and 13.8 cal mol^{-1} K^{-1}, respectively. Interestingly, the enthalpic and entropic destabilization approximately doubles when moving from a 3′-terminal mispair to an internucleotide mispair, and this observation likely has important implications for understanding why polymerases have substantial difficulty in extending beyond mispairs.

Previously, Goodman and co-workers (*11*) argued that polymerases can exploit differences in $\Delta G°$, $\Delta H°$, and $\Delta S°$ between correct and incorrect base pairs for nucleotide insertion, and the altered base pairing and stacking energy associated with mispair formation increases proportionately the apparent K_m for insertion of the incorrect nucleotide. A comparatively larger K_m for insertion of a modified nucleotide is associated with a stronger tendency for a candidate nucleotide to dissociate from the enzyme−primer−template complex.

Extension past a mispair, however, involves inserting a correct nucleotide, yet the K_m is also substantially higher than when extending past a correct pair. Upon comparison of the energetic penalty of mispair formation for the sequences examined here, it is apparent that an internucleotide mispair induces destabilization on both the 5′-side and the 3′-side of the mispair. At the misinsertion step, an incorrect base pair does not stack as well on the 5′-primer−template complex and is more likely to dissociate, resulting in an increased apparent K_m. At the extension step, an incoming correct nucleotide would stack, but only poorly, on the mispair. Thus, the destabilizing impact of the mispair is transmitted in the 3′-direction as well, perhaps explaining a significant component of polymerase extension fidelity.

Net Thermodynamic Differences between 3′-End Base Pairs and Internal Base Pairs Might Be Related to Ligase Efficiency. Upon comparison of thermodynamic parameters for base pairs located at the 3′-terminal position with those obtained for the same base pair located in an internucleotide position, some trends are apparent that could be important for understanding the activities of enzymes that act upon nucleic acids, including polymerases and ligases. The thermodynamic results presented here establish that the $U^{2'F(ribo)}$ substitution is more destabilizing, with larger magnitude $\Delta H°$ and $\Delta S°$ when on the 3′-end, relative to the internucleotide linkage. In contrast, $U^{2'F(ara)}$ is substantially less destabilizing than $U^{2'F(ribo)}$ on the 3′-end. However, upon comparison of the impact of $U^{2'F(ara)}$ substitution on the 3′-end to the internucleotide position, $U^{2'F(ara)}$ is more destabilizing in the internucleotide position than on the 3′-end. The conversion of the 3′-end modification to the internucleotide linkage could be accomplished by members of the DNA ligase family. Conversion of the 3′-end $U^{2'F(ara)}$ to an internucleotide linkage would increase the destabilizing impact of the substitution; however, conversion of the 3′-end $U^{2'F(ribo)}$ to an internucleotide linkage would substantially reduce the destabilizing impact of the substitution. We therefore predicted that the rate of ligation of the analogue substrates examined here would be as follows: A·$U^{2'F(ribo)}$ > A·dU > A·$U^{2'F(ara)}$.

The Relative Efficiency of DNA Ligases Is Consistent with Net Thermodynamic Differences on Synthetic Templates. Data obtained with *E. coli* DNA ligase and human

DNA ligase III, as shown in Figure 9, are consistent with the prediction given above, in that the order of ligase efficiency is as follows: $U^{2'F(ribo)} > dU > U^{2'F(ara)}$. As seen in the panel for the $U^{2'F(ara)}$ data, initial interaction of the ligase with the 5′-phosphate of the linker transfers an adenosine monophosphate group (App-5′-DNA). The same intermediate forms with both the $U^{2'F(ribo)}$ and dU substrates; however, with the $U^{2'F(ara)}$ substrate, the intermediate is less efficiently converted to the internucleotide linkage. Sugar pucker does impact ligase efficiency; however, the relative impact of the $U^{2'F(ara)}$ and $U^{2'F(ribo)}$ substitutions is opposite expectation based upon T_m values but likely explained by the thermodynamic differences described here. We note that previously, Mikita and Beardsley (*35*) observed that an oligonucleotide containing araC is ligated by T4 ligase 3 times more slowly than one with dC, although both oligonucleotides had similar T_m values. It was suggested that the presence of the 2′-OH in the arabino configuration could directly interfere with the ligase. In the studies reported here, the $A\cdot U^{2'F(ara)}$ base pair-containing oligonucleotide is ligated by human DNA ligase III approximately 4 times more slowly than the A·dU oligonucleotide. Likewise, the rate of ligation of the $A\cdot U^{2'F(ara)}$ oligonucleotide by *E. coli* DNA ligase is approximately 7 times slower than that of the A·dU oligonucleotide. Here, the difference in ligation rates is attributed to net thermodynamic differences between a 3′-end $A\cdot U^{2'F(ara)}$ base pair and the corresponding base pair in an internucleotide linkage. Although $U^{2'F(ara)}$ is less disruptive thermodynamically when placed at a duplex 3′-end, it is more disruptive thermodynamically when in an internucleotide linkage, perhaps accounting for decreased ligase efficiency.

In the ligase studies reported here, it was assumed that the primary effect of the 2′-F substitution was to constrain the sugar pucker equilibrium. It is important to note, however, that the larger fluorine substituent could induce additional steric effects as well as electronic effects upon the nucleophilicity of the 3′-OH, and these effects might be different for each isomer.

Net Thermodynamic Differences between 3′-End Base Pairs and Internal Base Pairs Might Be Related to Polymerase Extension Efficiency. Multiple studies on the impact of nucleotide analogues on polymerase incorporation and extension have been published (*7*, *8*, *34*−*41*). The various studies examining different sets of analogues and polymerases make it difficult to draw specific conclusions. However, one of the consistent findings, and unexplained paradoxes, with these nucleotide analogues is that some DNA polymerases strongly discriminate against ribonucleotides and 2′-deoxy-2′-fluoroarabino analogues at the insertion step but incorporate arabino and 2′-fluoro-2′-arabino analogues with kinetics similar to those of normal dNTPs. However, once incorporated, the arabino and 2′-deoxy-2′-fluoroarabino analogues prevent further elongation and act as chain terminators. In contrast, some DNA polymerases discriminate against ribonucleotides at insertion yet efficiently extend 3′-ribonucleotides. Indeed, DNA polymerase α preferentially adds dNTPs to ribonucleotide primers as part of the polymerase α−primase complex. Chain termination underlies the mechanism of toxicity for arabino analogues, yet the mechanism for the difference in polymerase preference between insertion and extension is unknown.

Above, we discussed surprising results with DNA ligase which revealed that the $U^{2'F(ara)}$ analogue was more thermodynamically destabilizing when in an internucleotide linkage as opposed to the 3′-end, and the net thermodynamic disadvantage with incorporating the 3′-OH of $U^{2'F(ara)}$ into an internucleotide linkage could provide an energetic barrier for polymerase extension. However, insufficient data currently exist to resolve this issue. Further studies are currently in progress to understand the role of sugar constraint on thermodynamic properties, and the results of these studies might provide mechanistic insights into the mechanism of action of an important class of antitumor and antiviral compounds.

REFERENCES

1. Petruska, J., Sowers, L. C., and Goodman, M. F. (1986) Comparison of nucleotide interactions in water, protein, and vacuum: Model for DNA polymerase fidelity. *Proc. Natl. Acad. Sci. U.S.A. 83*, 1559–1562.
2. Joyce, C. M., Sun, X. C., and Grindley, N. D. F. (1992) Reactions at the polymerase active site that contribute to the fidelity of *Escherichia coli* DNA polymerase I (Klenow Fragment). *J. Biol. Chem. 267*, 24485–24500.
3. Johnson, K. A. (1993) Conformational coupling in DNA polymerase fidelity. *Annu. Rev. Biochem. 62*, 685–713.
4. Goodman, M. F., and Fygenson, D. K. (1998) DNA polymerase fidelity: From genetics toward a biochemical understanding. *Genetics 148*, 1475–1482.
5. Beard, W. A., and Wilson, S. H. (2003) Structural insights into the origins of DNA polymerase fidelity. *Structure 11*, 489–496.
6. Joyce, C. M., and Benkovic, S. J. (2004) DNA polymerase fidelity: Kinetics, structure, and checkpoints. *Biochemistry 43*, 14318–14324.
7. Thompson, H. T., Sheaff, R. J., and Kuchta, R. D. (1995) Interactions of calf thymus DNA polymerase α with primer/templates. *Nucleic Acids Res. 23*, 4109–4115.
8. Richardson, F. C., Kuchta, R. D., Mazurkiewicz, A., and Richardson, K. A. (2000) Polymerization of 2′-Fluoro- and 2′-O-Methyl-dNTPs by human DNA polymerase α, polymerase γ, and primase. *Biochem. Pharmacol. 59*, 1045–1052.
9. Astatke, M., Grindley, M. D. F., and Joyce, C. M. (1998) How *E. coli* DNA polymerase I (Klenow fragment) distinguishes between deoxy- and dideoxynucleotides. *J. Mol. Biol. 278*, 147–165.
10. Marquez, V. E., Ben-Kasus, T., Barchi, J. J., Green, K. M., Nicklaus, M. C., and Agbaria, R. (2004) Experimental and structural evidence that herpes 1 kinase and cellular DNA polymerase(s) discriminate on the basis of sugar pucker. *J. Am. Chem. Soc. 126*, 543–549.
11. Petruska, J., Goodman, M. F., Boosalis, M. S., Sowers, L. S., Cheong, C., and Tinoco, I. (1988) Comparison between DNA melting thermodynamics and DNA polymerase fidelity. *Proc. Natl. Acad. Sci. U.S.A. 85*, 6252–6256.
12. Perrino, F. W., Preston, B. D., Sandell, L. L., and Loeb, L. A. (1989) Extension of mismatched 3′ termini of DNA is a major determinant of the infidelity of human immunodeficiency virus type 1 reverse transcriptase. *Proc. Natl. Acad. Sci. U.S.A. 86*, 8343–8347.
13. Zinnen, S., Hsieh, J.-C., and Modrich, P. (1994) Misincorporation and mispaired primer extension by human immunodeficiency virus reverse transcriptase. *J. Biol. Chem. 269*, 24195–24202.
14. Mendelman, L. V., Petruska, J., and Goodman, M. F. (1990) Base pair extension kinetics. Comparision of DNA polymerase α and reverse transcriptase. *J. Biol. Chem. 265*, 2338–2346.
15. Shah, A. M., Maitra, M., and Sweasy, J. B. (2003) Variants of DNA polymerase β extend mispaired DNA due to increased affinity for nucleotide substrate. *Biochemistry 42*, 10709–10717.
16. Altona, C., and Sundaralingam, M. (1972) Conformational analysis of the sugar ring in nucleosides and nucleotides. A new description using the concept of pseudorotation. *J. Am. Chem. Soc. 94*, 8205–8212.
17. Levitt, M., and Warshel, A. (1978) Extreme conformational flexibility of the furanose ring in DNA and RNA. *J. Am. Chem. Soc. 100*, 2607–2613.
18. Ferrin, L. J., and Mildvan, A. S. (1985) Nuclear overhauser effect studies of the conformations and binding site environments of deoxynucleoside triphosphate substrates bound to DNA polymerase I and its large fragment. *Biochemistry 24*, 6904–6913.
19. Harvey, S. C., and Prabhakaran, M. (1986) Ribose puckering: Structure, dynamics, energetics, and the pseudorotation cycle. *J. Am. Chem. Soc. 108*, 6128–6136.
20. Boulard, Y., Cognet, J. A., Gabarro-Arpa, J., Le Bret, M., Sowers, L. C., and Fazakerley, G. V. (1992) The pH dependent configurations of the C·A mispair in DNA. *Nucleic Acids Res. 20*, 1933–1941.
21. Cullinan, D., Johnson, F., Grollman, A. P., Eisenberg, M., and De Los Santos, C. (1997) Solution structure of a DNA duplex containing the exocyclic lesion 3, N4-etheno-2′-deoxycytidine opposite 2′-deoxyguanosine. *Biochemistry 36*, 11933–11943.

22. Allawi, H. T., and SantaLucia, J., Jr. (1998) NMR solution structure of a DNA dodecamer containing single G·T mismatches. *Nucleic Acids Res. 26*, 4925–4934.
23. Tonelli, M., and James, T. L. (1998) Insights into the dynamic nature of DNA duplex structure via analysis of nuclear Overhauser effect intensities. *Biochemistry 37*, 11478–11487.
24. Berger, I., Tereshko, V., Ikeda, H., Marquez, V. E., and Egli, M. (1998) Crystal structure of B-DNA with incorporated 2′-deoxy-2′-fluoro-arabino-furanosyl thymines: Implications of conformational preorganization for duplex stability. *Nucleic Acids Res. 26*, 2473–2480.
25. Damha, M. J., Wilds, C. J., Noronha, A., Brukner, I., Borkow, G., Arion, D., and Parniak, M. A. (1998) Hybrids of RNA and arabinonucleic acids (ANA and 2′F-ANA) are substrates of ribonuclease H. *J. Am. Chem. Soc. 120*, 12976–12977.
26. Ikeda, H., Fernandez, R., Wilk, A., Barchi, J. J., Jr., Huang, X., and Marquez, V. E. (1998) The effect of two antipodal fluorine-induced sugar puckers on the conformation and stability of the Dickerson-Drew dodecamer duplex $[d(CGCGAATTCGCG)]_2$. *Nucleic Acids Res. 26*, 2237–2244.
27. Wilds, C. J., and Damha, M. J. (1999) Duplex recognition by oligonucleotides containing 2′-deoxy-2′-fluoro-D-arabinose and 2′-deoxy-2′-fluoro-D-ribose. Intermolecular 2′-OH-phosphate contacts versus sugar puckering in the stabilization of triple-helical complexes. *Bioconjugate Chem. 10*, 299–305.
28. Schultz, R. G., and Gryaznov, S. M. (2000) Arabino-fluorooligonucleotide N3′ → P5′ phosphoramidates: Synthesis and properties. *Tetrahedron Lett. 41*, 1895–1899.
29. Wilds, C. J., and Damha, M. J. (2000) 2′-Deoxy-2′-fluoro-β-D-arabinonucleosides and oligonucleotides (2′F-ANA): Synthesis and physicochemical studies. *Nucleic Acids Res. 28*, 3625–3635.
30. Trempe, J.-F., Wilds, C. J., Denisov, A. Y., Pon, R. T., Damha, M. J., and Gehring, K. (2001) NMR solution structure of an oligonucleotide hairpin with a 2′F-ANA/RNA stem: Implications for RNase H specificity toward DNA/RNA hybrid duplexes. *J. Am. Chem. Soc. 123*, 4896–4903.
31. Kalota, A., Karabon, L., Swider, C. R., Viazovkina, E., Elzagheid, E., Damha, M. J., and Gewirtz, A. M. (2006) 2′-Deoxy-2′-fluoro-β-D-arabinonucleic acid (2′F-ANA) modified oligonucleotides (ON) effect highly efficient, and persistent, gene silencing. *Nucleic Acids Res. 34*, 451–461.
32. Peng, C. G., and Damha, M. J. (2007) G-Quadruplex induced stabilization by 2′-deoxy-2′-fluoro-D-arabinonucleic acids (2′F-ANA). *Nucleic Acids Res. 35*, 4977–4988.
33. Ziemkowski, P., Felczak, K., Poznanski, J., Kulikowski, T., Zielinski, Z., Ciesla, J., and Rode, W. (2007) Interactions of 2′-fluoro-substituted dUMP analogues with thymidylate synthase. *Biochem. Biophys. Res. Commun. 362*, 37–43.
34. Pinto, D., Sarocchi-Landousy, M.-T., and Guschlbauer, W. (1979) 2′-Deoxy-2′-fluorouridine-5′-triphosphates: A possible substrate for *E. coli* RNA polymerase. *Nucleic Acids Res. 6*, 1041–1048.
35. Mikita, T., and Beardsley, G. P. (1988) Functional consequences of the arabinosylcytosine structural lesion in DNA. *Biochemistry 27*, 4698–4705.
36. Kuchta, R. D., Ilsley, D., Kravig, K. D., Schubert, S., and Harris, B. (1992) Inhibition of DNA primase and polymerase α by arabinofuranosylnucleoside triphosphates and related compounds. *Biochemistry 31*, 4720–4728.
37. Perrino, F. W., and Mekosh, H. L. (1992) Incorporation of cytosine arabinoside monophosphate into DNA at internucleotide linkages by human DNA polymerase α. *J. Biol. Chem. 267*, 23043–23051.
38. Lewis, W., Meyer, R. R., Simpson, J. F., Colacino, J. M., and Perrino, F. W. (1994) Mammalian DNA polymerases α, β, γ, δ, and ε incorporate fialuridine (FIAU) monophosphate into DNA and are inhibited competitively by FIAU triphosphate. *Biochemistry 33*, 14620–14624.
39. Ono, T., Scalf, M., and Smith, L. M. (1997) 2′-Fluoro modified nucleic acids: Polymerase-directed synthesis, properties and stability to analysis by matrix-assisted laser desorption/ionization mass spectrometry. *Nucleic Acids Res. 25*, 4581–4588.
40. Perrino, F. W., Mazur, D. J., Ward, H., and Harvey, S. (1999) Exonucleases and the incorporation of aranucleotides into DNA. *Cell Biochem. Biophys. 30*, 331–352.
41. Richardson, K. A., Vega, T. P., Richardson, F. C., Moore, C. L., Rohloff, J. C., Tomkinson, B., Bendele, R. A., and Kuchta, R. D. (2004) Polymerization of the triphosphates of AraC, 2′,2′-difluorodeoxycytidine (dFdC) and OSI-7836 (T-araC) by human DNA polymerase α and DNA primase. *Biochem. Pharmacol. 68*, 2644–3647.
42. Tann, C. H., Brodfuehrer, P. R., Brundidge, S. P., Sapino, C., Jr., and Howell, H. G. (1985) Fluorocarbohydrates in synthesis. An efficient synthesis of 1-(2-deoxy-2-fluoro-β-D-arabinofuranosyl) thymine (β-FMAU). *J. Org. Chem. 50*, 3644–3647.
43. Howell, H. G., Brodfuehrer, P. R., Brundidge, S. P., Benigni, D. A., and Sapino, C., Jr. (1988) Antiviral nucleosides. A stereospecific, total synthesis of 2′-fluoro-2′-deoxy-β-D-arabinofuranosyl nucleosides. *J. Org. Chem. 53*, 85–88.
44. Martin, J. A., Bushnell, D. J., Duncan, I. B., Dunsdon, S. J., Hall, M. J., Machin, P. J., Merrett, J. H., Parkes, K. E. B., Roberts, N. A., Thomas, G. J., Galpin, S. A., and Kinchington, D. (1990) Synthesis and antiviral activity of monofluoro and difluoro analogues of pyrimidine deoxyribonucleosides against human immunodeficiency virus (HIV-1). *J. Med. Chem. 33*, 2137–2145.
45. Vaidyanathan, G., and Zalutsky, M. R. (1998) Preparation of 5-[^{131}I]iodo- and 5-[^{211}At]astato-1-(2-deoxy-2-fluoro-β-D-arabinofuranosyl) uracil by a halodestannylation reaction. *Nucl. Med. Biol. 25*, 487–496.
46. Hamamoto, S., and Takaku, K. (1986) New approach to the synthesis of deoxyribonucleoside phosphoramidite derivatives. *Chem. Lett.*, 1401–1404.
47. Gait, M. J. (1984) Oligonucleotide synthesis: A practical approach , Oxford, IRL Press, Washington, DC.
48. Cui, Z., Theruvathu, J. A., Farrel, A., Burdzy, A., and Sowers, L. C. (2008) Characterization of synthetic oligonucleotides containing biologically important modified bases by matrix-assisted laser desorption/ionization time-of-flight mass spectrometry. *Anal. Biochem. 379*, 196–207.
49. Connolly, B. A., and Newman, P. C. (1989) Synthesis and properties of oligonucleotides containing 4-thiothymidine, 5-methyl-2-pyrimidinone-1-β-D-(2′-deoxyriboside) and 2-thiothymidine. *Nucleic Acids Res. 17*, 4957–4974.
50. Pon, R. T., and Yu, R. (1997) Hydroquinone-*O*,*O*′-diacetic acid as a more labile replacement for succinic acid linkers in solid-phase oligonucleotide synthesis. *Tetrahedron Lett. 38*, 3327–3330.
51. Azhayev, A. V., and Antopolsky, M. L. (2001) Amide group assisted 3′-dephosphorylation of oligonucleotides synthesized on universal A-supports. *Tetrahedron 57*, 4977–4986.
52. Puglisi, J. D., and Tinoco, I., Jr. (1989) Absorbance melting curves of RNA. Methods in Enzymology (Dahlberg, J. E., and Abelson, E. N., Eds.) Vol. 180, pp 304−325, Academic Press, Orlando, FL.
53. SantaLucia, J., Jr., Allawi, H. T., and Seneviratne, P. A. (1996) Improved nearest-neighbor parameters for predicting DNA duplex stability. *Biochemistry 35*, 3555–3562.
54. Allawi, H. T., and SantaLucia, J., Jr. (1997) Thermodynamics and NMR of internal G·T mismatches in DNA. *Biochemistry 36*, 10581–10594.
55. Liu, P., Burdzy, A., and Sowers, L. C. (2004) DNA ligases ensure fidelity by interrogating minor groove contacts. *Nucleic Acids Res. 32*, 4503–4511.
56. Delort, A. M., Neumann, J. M., Molko, D., Herve, M., Teoule, R., and Tran, D. S. (1985) Influence of uracil defect on DNA structure: ^{1}H NMR investigation at 500 MHz. *Nucleic Acids Res. 13*, 3343–3355.
57. Carbonnaux, C., Fazakerley, G. V., and Sowers, L. C. (1990) An NMR structural study of deaminated base pairs in DNA. *Nucleic Acids Res. 18*, 4075–4081.
58. Sowers, L. C., Shaw, B. R., and Sedwick, W. D. (1987) Base stacking and molecular polarizability: Effect of a methyl group in the 5-position of pyrimidines. *Biochem. Biophys. Res. Commun. 148*, 790–794.
59. Aboul-ela, F., Koh, D., Tinoco, I., Jr., and Martin, F. H. (1985) Base-base mismatches. Thermodynamics of double helix formation for $dCA_3XA_3G + dCT_3YT_3G$ (X, Y = A, C, G, T). *Nucleic Acids Res. 13*, 4811–4824.
60. McTigue, P. M., Peterson, R. J., and Kahn, J. D. (2004) Sequence-dependent thermodynamic parameters for locked nucleic acid (LNA)-DNA duplex formation. *Biochemistry 43*, 5388–5405.